Neuron, Vol. 33, 439–452, January 31, 2002, Copyright ©2002 by Cell Press

The Life Cycle of Ca^{2+} Ions in Dendritic Spines

Bernardo L. Sabatini,[2] Thomas G. Oertner, and Karel Svoboda[1]
Howard Hughes Medical Institute
Cold Spring Harbor Laboratory
1 Bungtown Road
Cold Spring Harbor, New York 11724

Summary

Spine Ca^{2+} is critical for the induction of synaptic plasticity, but the factors that control Ca^{2+} handling in dendritic spines under physiological conditions are largely unknown. We studied [Ca^{2+}] signaling in dendritic spines of CA1 pyramidal neurons and find that spines are specialized structures with low endogenous Ca^{2+} buffer capacity that allows large and extremely rapid [Ca^{2+}] changes. Under physiological conditions, Ca^{2+} diffusion across the spine neck is negligible, and the spine head functions as a separate compartment on long time scales, allowing localized Ca^{2+} buildup during trains of synaptic stimuli. Furthermore, the kinetics of Ca^{2+} sources governs the time course of [Ca^{2+}] signals and may explain the selective activation of long-term synaptic potentiation (LTP) and long-term depression (LTD) by NMDA-R-mediated synaptic Ca^{2+}.

Introduction

Ca^{2+} ions play a crucial role in the induction of most forms of long-term synaptic potentiation (LTP) and long-term depression (LTD) (reviewed in Zucker [1999]), putative cellular models of learning and memory (Malenka and Nicoll, 1999). Postsynaptic Ca^{2+} accumulations are necessary to regulate enzymes that trigger rapid modifications of synaptic strength (Cummings et al., 1996) and also to activate transcription factors that facilitate long-term maintenance of synaptic modifications (Bito et al., 1997). Ca^{2+} also plays a role in short-term changes in membrane excitability (Storm, 1990) and synaptic structural plasticity (Engert and Bonhoeffer, 1999; Fischer et al., 2000; Maletic-Savatic et al., 1999; Toni et al., 1999). How can a single second messenger encode all of these functions? The answer must lie at least in part in the details: depending on differences in amplitude, spatial localization, and time course, different [Ca^{2+}] signals may carry very different biochemical meanings for the cell.

Ca^{2+} influx into dendritic spines is of particular importance to synaptic plasticity. The postsynaptic densities embedded in spine membranes contain many of the molecular Ca^{2+} sensors and their substrates that are involved in synaptic plasticity (Kennedy, 2000). Spines are tiny membranous compartments consisting of a head (volume $\sim$0.01–1 μm^3) connected to the parent dendrite via a thin (diameter $\sim$0.1 μm) spine neck (Harris and Kater, 1994). This peculiar structure limits diffusional exchange of signaling molecules, including Ca^{2+}, between spine heads, their parent dendrites, and neighboring spines (Holmes, 1990; Koch and Zador, 1993; Svoboda et al., 1996). Spines may therefore subserve biochemical compartmentalization necessary for input specificity in synaptic plasticity (Andersen et al., 1980).

Spine [Ca^{2+}] signals are shaped by the dynamics of Ca^{2+} sources and extrusion mechanisms, the properties and spatial distribution of Ca^{2+} buffers, and diffusion between dendrite and spine (reviewed in Sabatini et al. [2001]). Using high-resolution imaging techniques, the sources of spine [Ca^{2+}] have been explored under a variety of stimulation conditions. In pyramidal neurons, weak synaptic activation leads to postsynaptic Ca^{2+} influx primarily through NMDA-Rs (Koester and Sakmann, 1998; Kovalchuk et al., 2000; Yuste et al., 1999). Suprathreshold stimuli produce additional Ca^{2+} influx through VSCCs opened by backpropagating action potentials (Jaffe et al., 1992; Majewska et al., 2000b; Sabatini and Svoboda, 2000; Yuste and Denk, 1995). Under some conditions, Ca^{2+}-induced Ca^{2+} release (CICR) may also play a role (Emptage et al., 1999).

However, most [Ca^{2+}] measurements in spines have so far been performed with the help of high concentrations of Ca^{2+} indicators with high affinities for Ca^{2+}. Under these conditions, virtually every Ca^{2+} ion entering the cytoplasm binds the indicator, and interactions with endogenous buffers and extrusion mechanisms are perturbed, reducing the amplitude and prolonging the duration of [Ca^{2+}] transients. Not only are the *absolute* amplitude and time course of [Ca^{2+}] transients perturbed, but the *relative* differences between [Ca^{2+}] transients generated by different stimuli can also be distorted. For example, because of the long time course of NMDA-R-mediated Ca^{2+} currents compared with those produced by action potentials (AP), the NMDA-R-mediated [Ca^{2+}] transient will, compared with the AP-evoked one, appear relatively larger as more Ca^{2+} indicator is introduced. Furthermore, Ca^{2+} indicators diffuse rapidly in the cytoplasm while endogenous buffers are typically immobile or slowly mobile (Allbritton et al., 1992). The presence of Ca^{2+} indicators therefore enhances the spread of [Ca^{2+}] signals (Gabso et al., 1997) and renders interpretation of the role of Ca^{2+} diffusion through the spine neck in shaping [Ca^{2+}] transients (Majewska et al., 2000a, 2000b) problematic.

To explore the factors that normally regulate Ca^{2+} in spines and to uncover the features of stimulus-induced [Ca^{2+}] transients that determine whether synaptic plasticity is induced, measurements need to be performed in the presence of low exogenous buffer capacity. Furthermore, the perturbations due to the Ca^{2+} indicator need to be quantitatively taken into account. A conceptual framework for doing so has been developed (Neher and Augustine, 1992; Tank et al., 1995). A particularly useful variant of this method exploits the fact that the Ca^{2+} influx through VSCCs opened by action potentials is sufficiently short ($<$1 ms) to be considered instantaneous (Helmchen et al., 1996). Thus, AP-evoked [Ca^{2+}]

[1]Correspondence: svoboda@cshl.org
[2]Present address: Harvard Medical School, Department of Neurobiology, 220 Longwood Avenue, Boston, Massachusetts, 02215.

transients report the "impulse response" of a cellular compartment. Collecting measurements under conditions of varying indicator concentration and extrapolating back to the zero-added indicator condition yields information about Ca^{2+} handling in the native state of the neuron. Such an approach has been used to determine the amplitude and time course of AP-evoked [Ca^{2+}] transients and the endogenous Ca^{2+} buffering capacity in the main apical dendrite of pyramidal neurons (Helmchen et al., 1996; Maravall et al., 2000).

Here we use a similar technique to examine [Ca^{2+}] transients and handling in spines of hippocampal CA1 pyramidal neurons and show that spines are isolated, specialized Ca^{2+} compartments optimized for generating large free Ca^{2+} concentrations. For [Ca^{2+}] measurements, we use a method designed for robust [Ca^{2+}] estimation in small compartments (Maravall et al., 2000). This method makes no assumptions about resting [Ca^{2+}] and hence allows us to precisely determine [Ca^{2+}] in spines and dendrites despite possible heterogeneous resting Ca^{2+} levels. We find that the endogenous buffer capacity of spines and distal dendrites is small, and hence, [Ca^{2+}] transients in spines evoked by a single AP are unexpectedly large and brief in the absence of exogenous Ca^{2+} buffers. Furthermore, in unperturbed neurons, the spine head operates as a completely isolated compartment for the duration of AP-evoked transients. We also examined synaptically evoked [Ca^{2+}] transients and measured the amplitude and time course of NMDA-R-mediated transients in individual spines in resting and depolarized conditions. During these relatively long and large [Ca^{2+}] transients, endogenous Ca^{2+} buffers and extrusion pumps are not saturated. We find that, because of the rapid Ca^{2+} handling within spines, the kinetics of NMDA-R opening primarily determines the time course of synaptically evoked [Ca^{2+}] transients. Lastly, we discuss the importance of these findings for the induction of synaptic plasticity and propose that the kinetics of Ca^{2+} sources play a pivotal role in determining the induction of LTP and LTD.

Results

Action Potential-Evoked [Ca^{2+}] Transients

To measure the dynamics of intracellular free Ca^{2+} concentration, [Ca^{2+}], under conditions that minimize perturbation due to exogenous Ca^{2+} buffers, CA1 pyramidal cells in rat hippocampal slices were loaded with low concentrations (20 μM) of a green fluorescent calcium indicator ("green"; Fluo-4) through the patch pipette. Since these low levels of calcium indicator were too dim to reliably detect spines, we added a Ca^{2+}-insensitive fluorophore ("red"; Alexa fluor-594) to the pipette. Both fluorophores were efficiently two-photon excited at wavelengths of $\lambda = 810$ nm, and red fluorescence emitted by the Ca^{2+}-insensitive fluorophore was used to determine the dendritic morphology, while green fluorescence emitted by the Ca^{2+}-sensitive fluorophore was used to simultaneously measure [Ca^{2+}] dynamics (Figure 1).

We focused our measurements on small (diameter $<$ 2 μm) secondary to quaternary dendritic branches up to 150 μm from the soma (e.g., Figure 1A). In spines and their parent dendrites, fluorescence transients evoked

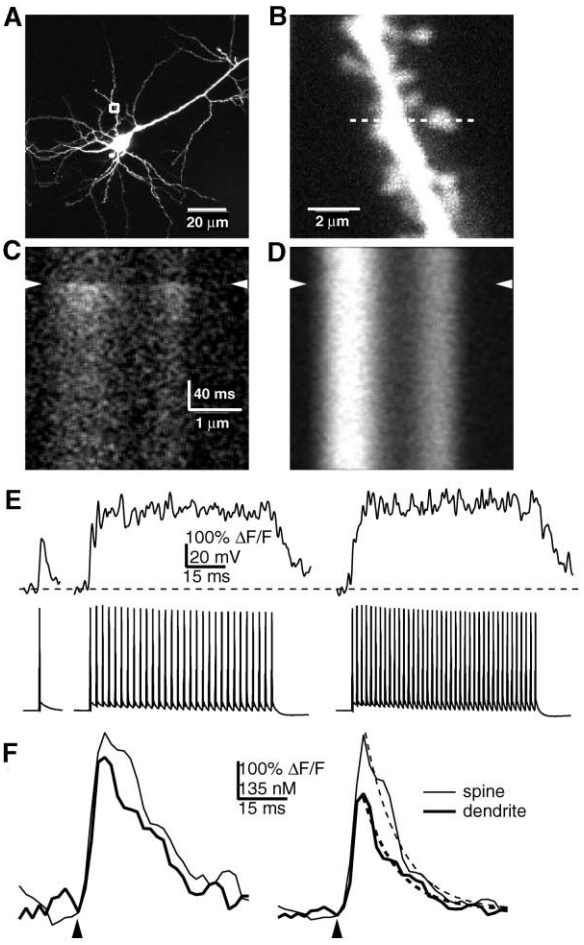

Figure 1. Imaging Action Potential-Evoked [Ca^{2+}] Dynamics in Dendrites and Spines

(A) Image of CA1 pyramidal neuron labeled with Fluo-4 and Alexa Fluor 594.

(B) Magnified image of a basal dendrite (boxed region in [A]).

(C and D) Linescan images over spine and parent dendrite (location of linescan indicated by dashed line in [B]). (C) green channel (Fluo-4) response to single action potential (arrow heads). (D) red channel (Alexa Fluor-594) recorded simultaneously.

(E) Green fluorescence transients in the spine evoked by a single action potential (left) or by trains at 62.5 (middle) or 83.3 (right) Hz (average of 15, 4, and 4 trials respectively).

(F) Average $(\Delta F/F)_{AP}$ (left) and $\Delta[Ca]_{AP}$ (right) in the spine (thin traces) and the neighboring dendrite (thick traces).

by single backpropagating action potentials, $(\Delta F/F)_{AP}$, were large and brief (Figures 1C, 1E, and 1F). To convert $(\Delta F/F)_{AP}$ to $\Delta[Ca]_{AP}$, we used a method (Maravall et al., 2000) that relies on determining the fluorescence that would arise from fully saturated indicator, $(\Delta F/F)_{max}$, without the need to make assumptions about resting [Ca^{2+}] (see Experimental Procedures). The value of $(\Delta F/F)_{max}$ was extrapolated from the plateau fluorescence reached during AP trains (Maravall et al., 2000) at 62.5 and 83.3 Hz (Figure 1E) and was used to determine Ca^{2+} concentration during the single AP-evoked transients in the spine and dendrite (Figure 1F). On average, $\Delta[Ca]_{AP}$ was large: 528 $\pm$ 251 nM in the spine and 401 $\pm$ 139 nM in the dendrite. [Ca^{2+}] returned to resting values quickly, and the decay phase in all cases was well fit by a single

exponential (Figure 1F). The time constant of decay to resting values (τ_{decay}) was determined from the single exponential fits and found to be 21 ± 10 ms in the spine and 27 ± 13 ms in the neighboring dendrite (n = 14 spines, 6 cells).

Depending on the relative buffer capacities of endogenous Ca^{2+} binding molecules and the Ca^{2+} indicator, even the low indicator concentrations used in Figure 1 could reduce $\Delta[Ca]_{AP}$ and slow the clearance of Ca^{2+} from the cytoplasm (see Experimental Procedures). Thus $\Delta[Ca]_{AP}$ under native conditions (i.e., without added Ca^{2+} indicators) could be even larger and briefer than reported above. The concentration and affinity for Ca^{2+} of the indicator determines its Ca^{2+} buffer capacity (κ_B) and hence the effect that the added indicator will have on $\Delta[Ca]_{AP}$ and the rate of Ca^{2+} clearance. κ_B is defined (Neher and Augustine, 1992) as the ratio of the number of Ca^{2+} ions that bind to the indicator to the number that remain free following a step increase in total Ca^{2+} (see Experimental Procedures) and is sometimes referred to as the "Ca^{2+} binding ratio." The amplitude of a [Ca^{2+}] transient is inversely proportional to the total Ca^{2+} buffer capacity (i.e., the sum of the endogenous and indicator buffer capacities), whereas the duration of the transient is directly proportional to the total Ca^{2+} buffer capacity (see Equations 3 and 4 in Experimental Procedures).

To infer [Ca^{2+}] dynamics in the absence of indicator, we measured $\Delta[Ca]_{AP}$ in spines of cells loaded with varying concentrations of several Ca^{2+} indicators (20 μM Fluo-4, n = 14 spines, 6 cells; 20 μM OGB1, n = 11 spines, 7 cells; 50 μM OGB1, n = 7 spines, 4 cells; and 100 μM OGB1, n = 10 spines, 8 cells). Resting Ca^{2+} concentrations ($[Ca]_0$), $\Delta[Ca]_{AP}$, τ_{decay}, and κ_B were determined and then averaged across spines for each indicator concentration. The low-affinity indicator Magnesium Green was also used for measurements of τ_{decay} (100 μM, n = 6 spines, 3 cells). Similar measurements were performed for the dendritic segments adjacent to the spine (Figures 1B–1D). $[Ca^{2+}]_0$ was similar in the spine (70 ± 29 nM, n = 28) and dendrite (65 ± 33 nM) and did not vary with the type of indicator used or indicator concentration (data not shown). Interestingly, these resting Ca^{2+} concentrations were significantly larger than those previously reported for the large proximal apical dendrites, ~40 nM (Maravall et al., 2000), using the same method. As expected, $\Delta[Ca]_{AP}$ decreased and τ_{decay} increased with higher indicator concentration and buffer capacity. Both $\Delta[Ca]_{AP}^{-1}$ and τ_{decay} were linearly related to κ_B (Figures 2A and 2B), and extrapolation to zero indicator concentration ($\kappa_B = 0$, the *y* axis intercept) gave $\Delta[Ca]_{AP}$ and τ_{decay} in unperturbed neurons. Under conditions of zero exogenous buffer, AP-evoked [Ca^{2+}] transients in spines and small dendrites are large and brief (in spines, $\Delta[Ca]_{AP}$ = 1.1 μM [0.6–8.2 μM] and τ_{decay} = 14 ms [12–20 ms]; in dendrites, $\Delta[Ca]_{AP}$ = 0.7 μM [0.4–2.0 μM] and τ_{decay} = 21 ms [6–36 ms]). The value given was measured from the best fit to the data and the range represents the 95% confidence interval of the fit.

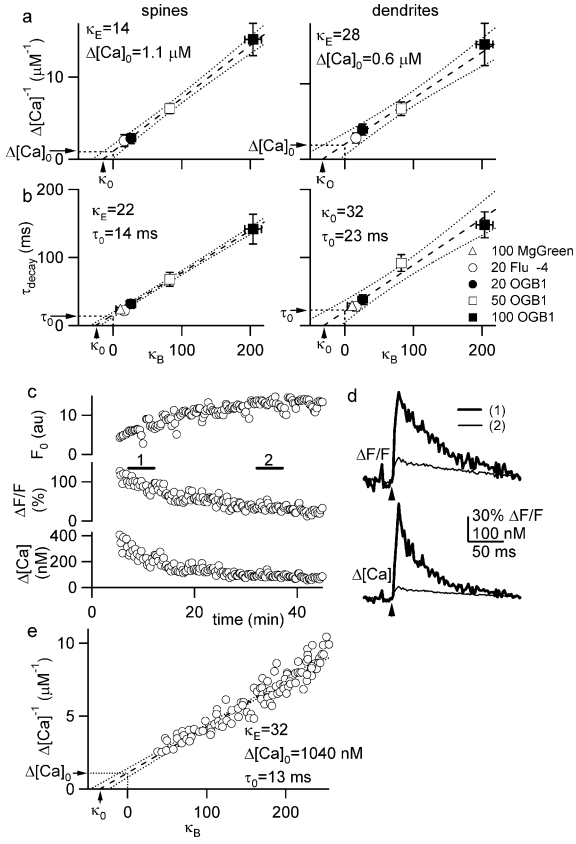

Figure 2. Effects of Added Buffer Capacity (κ_B) on Spine and Dendrite [Ca^{2+}] Dynamics

(A) Relationship between $\Delta[Ca^{2+}]_{AP}$ and added Ca^{2+} buffer capacity for spines (left) or dendrites (right) (avg ± SEM). Arrows indicate the calculated endogenous buffer capacity ($\kappa_E = -\kappa_0$) and $\Delta[Ca]_{AP}$ in the absence of added buffer ($\Delta[Ca]_0$) (see Equation 3 in Experimental Procedures). Experiments at different buffer levels were performed in separate spines.

(B) τ_{decay} as a function of added Ca^{2+} buffer capacity (same data set as in [A]). Arrows indicate the calculated endogenous buffer capacity and τ_{decay} in the absence of added buffer (τ_0). Dashed lines are the best linear fit to the data and the dotted lines are the 95% confidence bands of the fit.

(C) Resting fluorescence level (top), $(\Delta F/F)_{AP}$ (middle), and $\Delta[Ca]_{AP}$ (bottom) measured from an apical spine during loading of the cell with Ca^{2+} indicator. Time 0 indicates break-in into the cell. Bars and numbers correspond to traces displayed in (D).

(D) $(\Delta F/F)_{AP}$ (top) and $\Delta[Ca]_{AP}$ (bottom) from the spine measured early (thick, 1) or late (thin, 2) in loading as indicated in (C).

(E) $\Delta[Ca]_{AP}^{-1}$ plotted as a function of added Ca^{2+} buffer capacity. Arrows indicate the calculated endogenous buffer capacity (*x* axis) and $\Delta[Ca]_{AP}$ in basal conditions (*y* axis).

Endogenous Ca^{2+} Buffer Capacity in Small Dendrites and Their Spines

The relationship between $\Delta[Ca]_{AP}$ and κ_B provides insight about Ca^{2+} buffers in the cytoplasm in the absence of added buffers. We use the *x* axis intercepts (κ_0) of the fits in Figures 2A and 2B to measure the endogenous Ca^{2+} buffer capacity ($\kappa_E = -\kappa_0$) of spines and their parent dendrites (Helmchen et al., 1996). From the $\Delta[Ca]_{AP}^{-1}$ versus κ_B relationship we determined κ_E = 14 (2–31) in spines and κ_E = 28 (4–62) in the dendrite. The τ_{decay} versus κ_B relationship resulted in κ_E = 22 (18–33) in spines and κ_E = 32 (6–72) in the dendrite. These values of the endogenous buffer capacity are lower than those previously reported for the main apical dendrite (Helmchen et al., 1996; Maravall et al., 2000).

It is difficult to measure buffer capacities accurately

using measurements averaged over many structures, and variations between spines produce uncertainty in the extrapolation (Figures 2A and 2B) (Koester and Sakmann, 2000). To obtain more precise measurements, $\Delta[Ca]_{AP}$ and τ_{decay} were measured continuously in individual spines and their parent dendrites while a neuron was loaded with Ca^{2+} indicator (Figures 2C–2E). As the Ca^{2+} indicator entered the cell, $\Delta[Ca]_{AP}$ decreased and τ_{decay} increased in both the spine and dendrite (Figure 2C). Approximately 30–40 min after break-in, the indicator concentration in the spine and dendrite reached steady-state, and $\Delta[Ca]_{AP}$ remained constant after this point (Figure 2C). The increase in indicator concentration reduced $\Delta[Ca]_{AP}$ equally in spine and dendrite (ratio of decreases in spine over dendrite = 1.06 ± 0.19, n = 8), indicating that the endogenous Ca^{2+} buffer capacity was similar in these two compartments. The $\Delta[Ca]_{AP}^{-1}$ versus κ_B relationship obtained during filling of the cell with Ca^{2+} indicator was well fit by linear regression (Figure 2E), yielding low buffer capacities, κ_E = 24 ± 11 (range 12–37) in spines and κ_E = 27 ± 10 (range 19–42) in the neighboring parent dendrite (n = 5). This analysis also gave large values for $\Delta[Ca]_{AP}$, 1.7 ± 0.6 μM (range 1.0–2.6) and 1.5 ± 0.5 μM (range 0.9–2.4) in spines and dendrites of unperturbed neurons, respectively. Significant washout of mobile buffers during the recording would have resulted in a $\Delta[Ca]_{AP}^{-1}$ versus κ_B relationship that leveled off long after break-in (i.e., at high κ_B). Thus, the good linear fit of the $\Delta[Ca]_{AP}^{-1}$ versus κ_B relationship (Figure 2E) indicates that, as is the case in the proximal apical dendrites (Helmchen et al., 1996; Lee et al., 2000b), mobile Ca^{2+} buffers do not contribute significantly to Ca^{2+} buffering in spines and small dendrites. From the τ_{decay} versus κ_B relationship, τ_{decay} was found to be 12 ± 4 ms (range 8–16) in intact spines and 15 ± 5 ms (11–23) in the parent dendrite. Thus, after Ca^{2+} influx, approximately 5% of Ca^{2+} ions remain free while 95% are buffered by Ca^{2+} sequestration systems, and Ca^{2+} ions are rapidly removed from the spine cytoplasm with a time constant of τ_{decay} ~15 ms. Because of the near instantaneous rise in [Ca] caused by a single AP-evoked transients, τ_{decay} of AP-evoked [Ca^{2+}] transients is also a measure of the average lifetime of individual Ca^{2+} ions in the cytoplasm.

Role of Intracellular Stores in $\Delta[Ca]_{AP}$

Rapid removal of Ca^{2+} from the cytoplasm could occur by extrusion to the extracellular space as well as into intracellular stores. We measured the relative contribution of transport of Ca^{2+} ions into intracellular stores by abolishing transport into the smooth endoplasmic reticulum (SER) by blocking the SER Ca^{2+} ATPase (SERCA) pumps with CPA (Figure 3A). After application of CPA, τ_{decay} increased by approximately 50% in both spines (range 8%–110%, n = 4) and dendrites (range 20%–70%) (Figure 3B), indicating that Ca^{2+} uptake into the SER plays a role in Ca^{2+} clearance from spines. The amplitudes of $\Delta[Ca^{2+}]_{AP}$ in spines and dendrites were not affected by CPA application (Figure 3C), confirming that $\Delta[Ca]_{AP}$ is due to Ca^{2+} entering the cell through VSCCs (Sabatini and Svoboda, 2000; Yuste and Denk, 1995) without significant contribution from Ca^{2+}-induced Ca^{2+} release (CICR) (Emptage et al., 1999; Mainen et al., 1999).

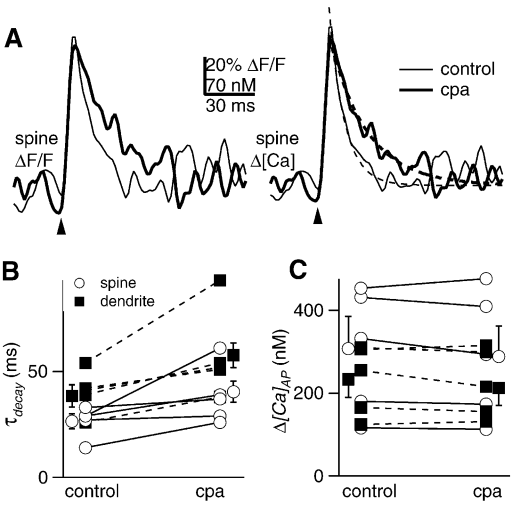

Figure 3. Block of Ca^{2+} Uptake into Intracellular Stores Prolongs AP-Evoked [Ca^{2+}] Transients

(A) $(\Delta F/F)_{AP}$ (left) and $\Delta[Ca]_{AP}$ (right) transient in a spine before (thin) and after (thick) addition of 30 μM CPA.

(B) Summary of effects of CPA on τ_{decay} in spines (open circles) and parent dendrites (closed squares). The effects of CPA were highly variable, probably reflecting the fact that only a subset of spines contains SER (Spacek and Harris, 1997).

(C) Effects on $\Delta[Ca]_{AP}$. The averages for each population are shown to the left and right of the group data.

Diffusional Coupling between Spine Head and Dendrite

The rapid clearance of Ca^{2+} from the cytoplasm and the slow diffusion of Ca^{2+} bound to endogenous buffers (Allbritton et al., 1992) suggests that the spine head and neighboring dendrite might operate as completely separate Ca^{2+} signaling compartments. This is supported by the observation that in many spines loaded with low concentrations of Ca^{2+} indicator, Ca^{2+} gradients across the spine neck persisted for the entire duration of AP-evoked [Ca^{2+}] transients (e.g., Figure 1F). Diffusional coupling between spine and dendrite is further constrained by the narrow spine neck, which poses a diffusional barrier that is expected to depend on the length and diameter of the spine neck as well as the size of the spine head. Since morphology varies greatly among spines (Harris and Kater, 1994) (Figures 4A and 4B), it is possible that the efficacy of diffusional coupling of the spine head to the dendrite is similarly diverse. Since previous measurements of diffusional coupling between spine heads and dendrites have used fluorescence recovery after photobleaching (Majewska et al., 2000a, 2000b; Svoboda et al., 1996), a technique that has a likelihood of inducing photodamage, we developed an alternative approach. We measured the time course of diffusional equilibration of calcium (τ_{equi}) across the spine neck using fluctuation analysis of $\Delta[Ca]_{AP}$ in cells loaded with 100 μM Fluo-4 (Sabatini and Svoboda, 2000). Because of the stochastic nature of VSCC opening, the gradient in [Ca^{2+}] across a spine neck following an action potential will vary from trial to trial. These gradients are dissipated by diffusion of Ca^{2+} across the spine neck, and the time constant of diffusonal coupling is reflected

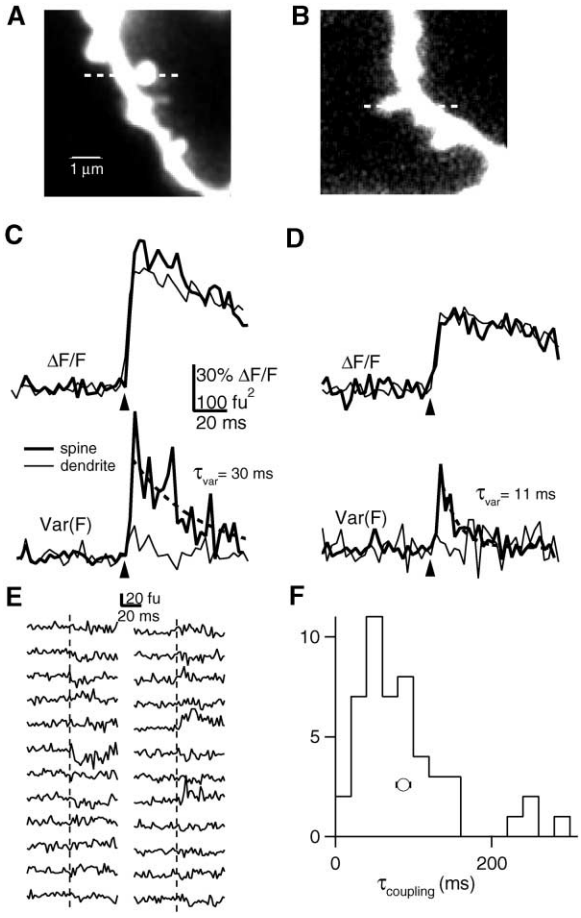

Figure 4. Diffusional Equilibration of Ca^{2+} across the Spine Neck Measured with Optical Fluctuation Analysis

(A and B) Examples of dendritic spines.

(C) Average $(\Delta F/F)_{AP}$ (top, 66 trials) in the spine (thick) and parent dendrite (thin) for spine shown in (A). The variance of the fluorescence transients due to fluctuations in $[Ca^{2+}]$ in the spine and dendrite are shown below. Superimposed is an exponential fit to the decay of the variance in the spine (dashed line).

(D) Average $(\Delta F/F)_{AP}$ (top, n = 50) and variance of the fluorescence transient due to fluctuations in $[Ca^{2+}]$ (bottom) for the spine and parent dendrite shown in (B).

(E) Deviations from the mean for 24 sequential trials of $(\Delta F/F)_{AP}$. Dashed lines indicate the time of somatic current injection.

(F) Histogram of τ_{equi} measured from 49 spine/dendrite pairs. The mean $\tau_{equi} \pm$ SEM is also indicated.

in the time constant of decay of the trial-to-trial variance in action potential-evoked $[Ca^{2+}]$ transients.

The mean fluorescence transient and trial-to-trial variance in fluorescence due to fluctuations in intracellular Ca^{2+} ($\sigma_{F,Ca}^2$) were calculated (see Experimental Procedures) in spines and the neighboring parent dendrite (Figures 4C and 4D). $\sigma_{F,Ca}^2$ was larger in spines than in dendrites due to the smaller surface area of the spine and the smaller number of VSCCs that contribute to Ca^{2+} influx into the spine (Sabatini and Svoboda, 2000). A large $\sigma_{F,Ca}^2$ in the spine and a small or no $\sigma_{F,Ca}^2$ in the dendrite are evidence of a diffusion barrier posed by the spine neck; without such a barrier, Ca^{2+} would equilibrate quickly across the spine neck and hence trial-to-trial variability should be equal in both compartments. Interestingly, differences in $\sigma_{F,Ca}^2$ between the spine and neighboring dendrite, caused by concentration gradients during *individual* AP-evoked $[Ca^{2+}]$ transients, were seen in spines/dendrite pairs that showed no gradients in *average* $\Delta[Ca]_{AP}$ (Figures 4C and 4D). Individual measurements of $(\Delta F/F)_{AP}$ in the spine showed large and long lasting deviations from the mean $(\Delta F/F)_{AP}$ (Figure 4E).

The decay of the variance in the spine, $\sigma_{F,Ca}^2$, was well fit by a single exponential (time constant τ_{var}) and occurred faster than the decay of $(\Delta F/F)_{AP}$ (Figures 4C and D). It can be shown that τ_{var} is related to τ_{equi} such that $\tau_{equi} \geq 2\tau_{var}$ (see Experimental Procedures). τ_{equi} varied according to spine morphology (Figures 4A and 4C versus 4B and 4D) and was on average 89 $\pm$ 31 ms (range 12–190, n = 49) (Figure 4F), consistent with previous measurements (Svoboda et al., 1996). Because of the rapid mobility of Ca^{2+} indicators in the cytoplasm relative to endogenous Ca^{2+} binding proteins, τ_{equi} measured by this method underestimates by a factor of 10–100 (Allbritton et al., 1992) the time constant of diffusional equilibration across the spine neck in neurons without added indicator, suggesting that Ca^{2+} is compartmentalized for >1 s in unperturbed spines. Since τ_{equi} is long compared to the residence time of Ca^{2+} ions in the cytoplasm ($\tau_{decay} \sim$15 ms), diffusional exchange between spine and dendrite is unlikely to be an important determinant of $[Ca^{2+}]$ dynamics in spines in unperturbed neurons.

Synaptically Evoked $[Ca^{2+}]$ Transients

The lifetime of Ca^{2+} ions in the spine cytoplasm measured following the near instantaneous Ca^{2+} influx produced by APs may not be directly relevant to the larger and longer Ca^{2+} influx produced by synaptic NMDA-R activation. Synaptic $[Ca^{2+}]$ transients could overload the Ca^{2+} pumps and therefore lead to slower extrusion rates and longer Ca^{2+} ion lifetimes. On the other hand, high $[Ca^{2+}]$ levels might recruit additional extrusion mechanisms and shorten Ca^{2+} ion lifetimes. Such stimuli could also saturate buffers or alternatively be selectively more sensitive to Ca^{2+} buffers with slow on rates; thus, the effective endogenous buffer capacities shaping synaptic $[Ca^{2+}]$ transients could be larger or smaller than those shaping AP-evoked transients. To determine if the insights gained about Ca^{2+} handling with brief currents, such as those produced by action potentials, apply to synaptic $[Ca^{2+}]$ signaling (linearity), we measured the time course of NMDA-R-mediated $[Ca^{2+}]$ transients and compared them to the time course of NMDA-R-mediated synaptic currents. Since the shape of the AP-evoked $[Ca^{2+}]$ transient represents the response of the system to an instantaneous infusion of Ca^{2+}, if linearity holds the shape of the NMDA-R-mediated $[Ca^{2+}]$ transient, it is expected to equal the convolution of the AP-evoked $[Ca^{2+}]$ transient with the NMDA-R-mediated synaptic current.

Stimulation of presynaptic fibers that formed synapses onto imaged spines produced increases in green fluorescence that were confined to the spine head (Figure 5A). Fluorescence changes were quantified by measuring fluorescence in a line scan that intersected the spine head and dendrite (Figure 5B) during synaptic stimulation. To achieve a fluorescence signal evoked by

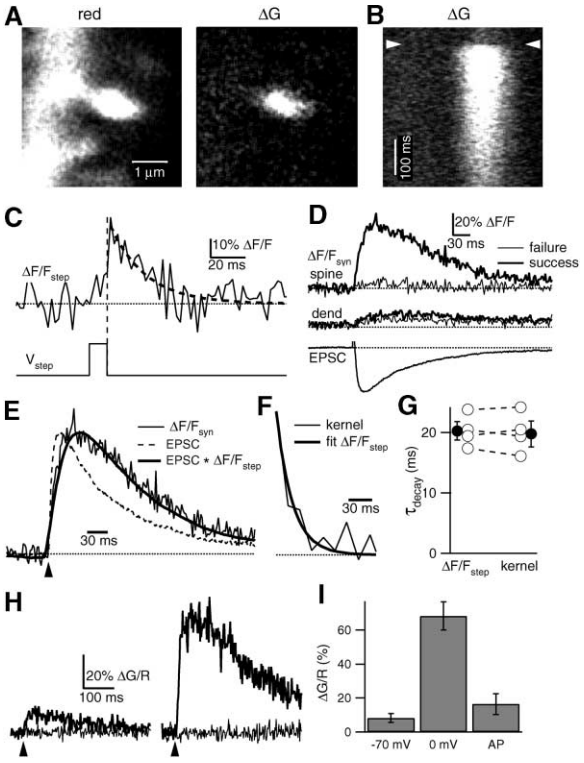

Figure 5. Time Course of Synaptically Evoked [Ca^{2+}] Transients through NMDA-Type Glutamate Receptors

(A) Red fluorescence (left) and $(\Delta F/F)_{syn}$ (right) for an apical spine following synaptic stimulation.

(B) Green fluorescence in line scan over dendrite and spine shown in (A) during synaptic stimulation (arrowhead).

(C) $(\Delta F/F)_{step}$ (top) measured in a spine following a 10 ms step from −70 mV to +50 mV delivered at the soma (bottom).

(D) Average $(\Delta F/F)_{syn}$ in the spine (top) and dendrite (middle) during success and failures and the EPSC measured at the soma (bottom).

(E) Comparison of the time course of $(\Delta F/F)_{syn}$, the EPSC, and the convolution of the EPSC with exponential fit to the decay of $(\Delta F/F)_{step}$.

(F) Comparison of time constants of decay of $(\Delta F/F)_{step}$ and of the convolution kernel.

(G) Change of green fluorescence over red fluorescence ($\Delta G/R_{syn}$) for a single success (thick) and failure (thin) trials at a holding potential of −70 (left) and 0 mV (right).

(H) Average $\Delta G/R_{syn}$ at −70 and 0 mV and $\Delta G/R_{AP}$.

synaptic stimulation ($(\Delta F/F)_{syn}$) that is proportional to the synaptically evoked NMDA-R [Ca^{2+}] transient ($\Delta[Ca]_{syn}$), it is important to use a low-affinity Ca^{2+} indicator that is not saturated by synaptic [Ca^{2+}] transients. Thus we recorded $(\Delta F/F)_{syn}$ in cells loaded with 100 μM Magnesium Green ($K_D \approx 6$ μM). Since we wanted to manipulate the postsynaptic potential to relieve the Mg^{2+} block of NMDA-Rs, Cs^+-based internal solutions and whole-cell voltage clamp were used. Since under these conditions action potentials cannot be evoked, the [Ca^{2+}] response to short Ca^{2+} currents was determined using Ca^{2+} tail currents (Figure 5C). On repolarization to −70 mV following a 10 ms step to +50 mV, $\Delta F/F$ ($(\Delta F/F)_{step}$) increased quickly (<2 ms, the time resolution of our measurements) and then decreased with a time constant of 20 ± 4 ms, consistent with the time constant observed in response to action potentials under similar buffer loading (Figure 1).

$(\Delta F/F)_{syn}$ was subsequently measured in the same spines at a holding potential of 0 mV, and in interleaved trials, the NMDA-R-mediated EPSC was recorded at the soma by hyperpolarizing the neuron slightly (−10 mV) (Figure 5D). Trials in which neurotransmitter was released ("success" trials) could be distinguished from trials in which no release occurred ("failure" trials) (Figure 5D), and on average, for success trials at 0 mV, $(\Delta F/F)_{syn} = 57\%$ (n = 4 spines, 10–50 trials/spine, range 36%–69%).

As expected, $(\Delta F/F)_{syn}$ had rising and falling phases that were slower than those of either the EPSC or $(\Delta F/F)_{step}$. The time course of $(\Delta F/F)_{syn}$ was well fit by the convolution of the EPSC and the decay phase of $(\Delta F/F)_{step}$ (Figure 5E). Similarly, the deconvolution of $(\Delta F/F)_{syn}$ by the EPSC resulted in a convolution kernel whose time course matched the decay phase of $(\Delta F/F)_{step}$ (Figure 5F). Thus, the "impulse response" of the spine is the same during AP-evoked, tail current-evoked, and NMDA-R-mediated [Ca^{2+}] transients; and the residence time of Ca^{2+} ions in the spine is essentially identical during these [Ca^{2+}] signals of varying amplitudes and durations. Hence, Ca^{2+} extrusion and buffering mechanisms are neither saturated nor facilitated during the large and long-lived NMDA-R-mediated transient. Furthermore, since the time course of synaptically evoked [Ca^{2+}] transients is purely determined by the time course of NMDA-R opening and the rapid kinetics of Ca^{2+} clearance, CICR does not contribute to the Ca^{2+} accumulation.

What is the amplitude of NMDA-R-mediated $\Delta[Ca]_{syn}$ under conditions of relieved Mg^{2+} block? Using low-affinity Ca^{2+} indicators did not allow us to convert $(\Delta F/F)_{syn}$ to $\Delta[Ca]_{syn}$ directly since the indicator could not be saturated reliably (Maravall et al., 2000) (see Experimental Procedures). Instead we compared $(\Delta F/F)_{syn}$ with $(\Delta F/F)_{AP}$ measured in spines of separate neurons in the presence of the same Ca^{2+} indicator in a K^+-based internal solution. In these conditions, $(\Delta F/F)_{AP} = 7.1\%$ (range 3.5–9.9, n = 6; and data not shown); therefore, the amplitude of the synaptic [Ca^{2+}] transient is ~8-fold larger than the amplitude of the AP-evoked transient. Since neither Ca^{2+} extrusion mechanisms nor Ca^{2+} buffers were saturated by NMDA-R-mediated transients, we can use this ratio and the amplitude of AP-evoked [Ca^{2+}] transients at zero-added buffer conditions (~1.5 μM) to conclude that NMDA-R-mediated transients in unperturbed spines at depolarized potentials reach amplitudes of ~12 μM.

NMDA-R-mediated Ca^{2+} influx at resting potentials is a trigger for LTD, whereas, when coupled with postsynaptic depolarization, it triggers LTP. Could this difference be explained by large differences in the amplitude of Ca^{2+} influx? We examined the relative size of $\Delta[Ca]_{syn}$ at −70 and 0 mV in cells loaded with 20 μM Alexa-594 and 300 μM of the Ca^{2+} indicator Fluo-5F ($K_D \approx 800$ nM) in a Cs^+-based intracellular solution (Figure 5G). A measure of relative Ca^{2+} increases was obtained by calculating the increase in green fluorescence from resting levels normalized by the total red fluorescence ($(\Delta G/R)_{syn}$). In addition, the resting green to red ratio (G/R_0) provides a measure proportional to $[Ca]_0$. Success trials were clearly distinguishable from failures at holding potentials of both −70 and 0 mV (Figure 5H). Success trials were averaged to yield peak $(\Delta G/R)_{syn}^{0\ mV} = 0.68$ (range 0.61–0.80) and $(\Delta G/R)_{syn}^{-70\ mV} = 0.08$ (range 0.05–0.11) (n =

4). In all spines, $(\Delta G/R)_{syn}$ was larger at 0 mV than at −70 mV (average 8.8-fold, range 7.1–12.8), reflecting relief of extracellular Mg^{2+} block of the NMDA-R at depolarized potentials (Figure 5I). This ratio may underestimate the differences in Ca^{2+} influx at resting and depolarized potentials due to saturation of the indicator during the larger $[Ca^{2+}]$ transients. In separate experiments using the same dye combination and a K^+-based intracellular solution, $(\Delta G/R)_{AP}$ was measured ($(\Delta G/R)_{AP} = 0.17$ [range 0.1–0.25], n = 4) and compared to $(\Delta G/R)_{syn}$ (Figure 5H). Thus, using $\Delta[Ca]_{AP}$ in zero-added buffer (∼1.5 μM) as a yardstick, we calculate that $\Delta[Ca]_{syn}^{-70\ mV}$ is ∼700 nM (1.5 μM × $(\Delta G/R)_{syn}^{-70\ mV}/(\Delta G/R)_{AP}$). Lastly, $[Ca]_0$ was ∼60% higher at 0 mV than −70 mV, possibly due to increased baseline Ca^{2+} influx at the depolarized potentials ($(G/R)_0^{-70\ mV} = 0.12$ [range 0.08–0.14] versus $(G/R)_0^{0\ mV} = 0.19$ [range 0.14–0.28]).

Discussion

Ca^{2+} Handling in Spines during Action Potentials

We find that spines and small dendrites are specialized cellular structures designed for large and brief $[Ca^{2+}]$ signals. A single action potential raises $[Ca^{2+}]$ in the spine to ∼1.5 μM (Figure 2). This large increase is due to influx through VSCCs, without contribution from CICR (Figure 3) and is possible because of the low endogenous buffer capacity of the spine (∼20, Figure 2). Thus, the total AP-evoked Ca^{2+} influx into a spine is on the order of 30 μM, of which, ∼5% stays free and the remainder binds to endogenous Ca^{2+} buffers (Figure 6A). For a spine with a volume of 0.1 fl this corresponds to ∼2000 Ca^{2+} ions entering through VSCCs and ∼100 remaining free in the cytoplasm. Other neuronal compartments show much larger buffer capacities, including main apical dendrites of pyramidal neurons (60–100 [Helmchen et al., 1996; Maravall et al., 2000]), small dendritic branches and axonal boutons of pyramidal neurons (Koester and Sakmann, 2000), apical dendrites of cerebellar Purkinje cells (2000 [Fierro and Llano, 1996]), and crayfish neuromuscular junction terminals (600 [Tank et al., 1995]). Comparing measurements of κ_E by different groups is complicated by uncertainties in the Ca^{2+} affinity of the indicator used. The value determined for κ_E depends on the Ca^{2+} affinity of the indicator used, such that $\kappa_E \propto 1/K_D$ (combining Equations 1 and 2 in Experimental Procedures). However, we have previously measured κ_E in proximal apical dendrites of CA1 pyramidal neurons using the techniques and indicator as in Figure 3 and found $\kappa_E = 65 \pm 15$ (Maravall et al., 2000). Thus, in CA1 pyramidal neurons, there exists a >3-fold difference in Ca^{2+} buffering capacity from proximal apical dendrite to distal dendrites and spines, reflecting local specialization of Ca^{2+} handling and a possible differential distribution of Ca^{2+} binding proteins within the cell. Similar to previous results for the main apical dendrite of pyramidal neurons (Helmchen et al., 1996; Lee et al., 2000b), we found no evidence for rapidly mobile Ca^{2+} buffers that washout of spines and distal dendrites during a typical recording (∼1 hr) session.

Can the large Ca^{2+} accumulations in spines be explained by their large surface-to-volume ratios (*SVR*)? *SVR* decreases in proportion to radius and spines have

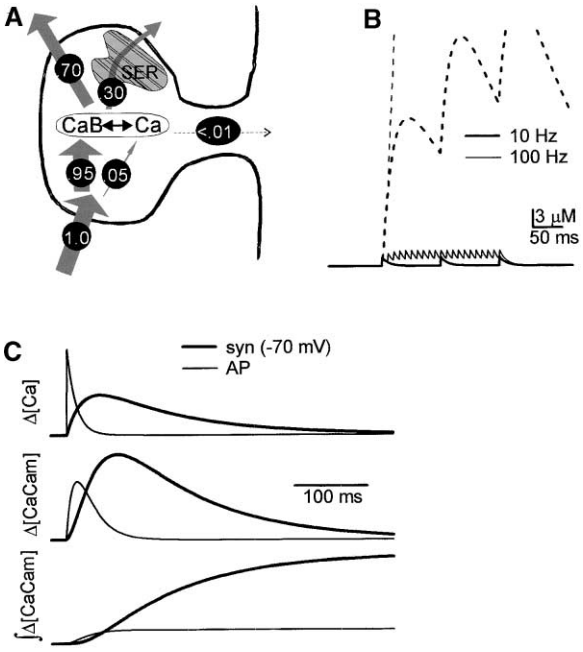

Figure 6. Simulation of Ca^{2+} Accumulation and Calmodulin Activation in Spines

(A) Schematic of Ca^{2+} handling in a typical dendritic spine. Arrows show pathways of Ca^{2+} flux, and the associated numbers show the fraction of Ca^{2+} handled by a particular pathway. Of the Ca^{2+} entering through Ca^{2+}-permeable channels, 95% binds to endogenous buffers and 5% stays free. 70% of Ca^{2+} extrusion occurs directly across the plasma membrane, whereas 30% passes through the SER. A negligible fraction diffuses from the spine head to the dendrite.

(B) Ca^{2+} accumulation during trains of action potentials (solid lines) or synaptic stimulation at 0 mV (dashed lines) at 10 (thick) and 100 (thin) Hz for 200 ms.

(C) $\Delta[Ca^{2+}]$ (top), activated calmodulin accumulation (middle), or total calmodulin activation (bottom) following an action potential (thin) or synaptic stimulation at −70 mV (thick).

SVRs approximately 5- to 10-fold greater than apical dendrites (Table 1). Thus, assuming uniform density of VSCCs in the cell membrane, AP-evoked $[Ca^{2+}]$ transients in spines should be ∼5- to 10-fold larger than in the main apical dendrite because of differences in *SVR,* and a further ∼2- to 3-fold larger because of the lower endogenous buffer capacity in spines. Comparing this calculation with measurement of $\Delta[Ca]_{AP}$ in spines (1.7 μM) and dendrites (200 nM) (Helmchen et al., 1996; Maravall et al., 2000) shows that differences in *SVR* and κ_E alone could account for differences in Ca^{2+} accumulations, without a need to postulate hotspots of VSCCs in spines.

Spine Ca^{2+} is rapidly extruded from the cytoplasm and, in unperturbed conditions, returns to resting levels with a time constant of ∼12 ms (Figure 2). This decay time is faster than for any $[Ca^{2+}]$ signal previously described in other neuronal compartments (Helmchen et al., 1996; Maravall et al., 2000; Tank et al., 1995) and approaches the rapid clearance of Ca^{2+} in fast-twitch skeletal muscle (Hollingworth et al., 1996). In spines and dendrites of cerebellar Purkinje neurons, Ca^{2+} decays are biphasic with a rapid component nearly as fast as that described here (Miyakawa et al., 1992; Wang et al.,

Table 1. Properties of $[Ca^{2+}]$ Transients and Handling Mechanisms in Spines, Small Dendrites, and the Main Apical Dendrite of Pyramidal Neurons

Structure	Radius (μm)	SVR (μm^{-1})	$\Delta[Ca^{2+}]_{AP}$ (μM)	$\Delta[Ca^{2+}]_{NMDA}$ (0 mV)	$\Delta[Ca^{2+}]_{NMDA}$ (−70 mV)	κ	γ (s^{-1})	τ_{decay} (ms)
Spines	0.1–0.5	4–20	1.7	12	0.7	20	1600	12
Small Dendrite	0.5–2	1–4	1.5	NA	NA	20	1200	15
Large Apical Dendrite	3–5	0.4–0.7	0.2	NA	NA	60–100	600–1000	100

Data are from this paper and Helmchen et al. (1996) and Maravall et al. (2000).

2000); however, the rapid component is a consequence of the nonlinear behavior of a saturable or kinetically slow Ca^{2+} buffer (Maeda et al., 1999).

Is the rapid decay time of $[Ca^{2+}]$ signals in spines due to specialized extrusion mechanisms? In a compartment without exogenous Ca^{2+} buffers,

$$\tau_{decay} = \frac{1 + \kappa_E}{\gamma} \propto \frac{1 + \kappa_E}{J(SVR)},$$

where κ_E is the endogenous buffer capacity, γ is the Ca^{2+} clearance rate constant, and J is the Ca^{2+} extrusion flux (γ/membrane area). From our data, $\gamma \approx 1600\ s^{-1}$, and the ratio of Ca^{2+} extrusion fluxes in a proximal dendrite ($r = 2.5\ \mu m$) to that of the spine ($r = 0.25\ \mu m$) is

$$\frac{J_{prox}}{J_{spine}} \approx \frac{\kappa_E^{prox}}{\kappa_E^{spine}} \frac{\tau_{decay}^{spine}}{\tau_{decay}^{prox}} \frac{SVR^{spine}}{SVR^{prox}} \approx 3 - 5,$$

using values given in Table 1. Thus, the Ca^{2+} extrusion flux is actually lower in distal dendrites and spines than close to the soma, and the remarkably rapid clearance of Ca^{2+} from these structures is primarily attributable to the small size of spines (and consequently the large *SVR*) and low endogenous buffer capacity.

What are the mechanisms of Ca^{2+} extrusion from dendritic spines? We find that ~30% of the Ca^{2+} clearance is by sequestration into internal stores via SERCA (Figures 3 and 6A). However, the effects of blocking intracellular stores on Ca^{2+} extrusion rates from spines were highly variable (Figure 3B), possibly reflecting the variable presence of spine apparatuses in spine heads (Spacek and Harris, 1997). The remainder of the Ca^{2+} extrusion could be through the plasma membrane Ca^{2+} ATPase (PMCA) or via the Na^+/Ca^{2+} exchanger. PMCA is a low-capacity, high-affinity ($K_m \approx 200$ nM) pump, which would be saturated by the large transients (Guerini and Carafoli, 1999) seen here following a single AP or synaptic stimulation. Therefore, the relatively higher capacity and lower affinity Na^+/Ca^{2+} exchanger (Philipson, 1999) is most likely responsible for the majority of Ca^{2+} efflux from the spine.

Ca^{2+} Handling in Spines during Synaptic Stimulation

Ca^{2+} currents evoked by action potentials are brief (< 1 ms) and relatively small (Figure 1) whereas synaptically evoked NMDA-R currents with Mg^{2+} block relieved are much longer (> 100 ms) and larger (Figure 5). Since the total Ca^{2+} influx evoked by synaptic stimulation is orders of magnitude larger than during action potentials, it could be possible for synaptic Ca^{2+} to saturate endogenous Ca^{2+} buffers and extrusion mechanisms. Alternatively, the long time course of synaptic Ca^{2+} influx might allow kinetically slow Ca^{2+} binding proteins (Lee et al., 2000a, 2000b) to sequester a larger fraction of the Ca^{2+} influx following synaptic stimulation compared to AP stimulation. Instead, we found that Ca^{2+} buffering and the kinetics of Ca^{2+} extrusion are the same for all conditions probed. During longer trains of stimuli, Ca^{2+} clearance is apparently slowed and a nonlinear component of Ca^{2+} dynamics is revealed (R.Y., B.S., and K.S., unpublished data). Over the large range of current amplitudes and durations explored here, $[Ca^{2+}]$ transients behave linearly in the sense that their time course is the convolution of the time course of the Ca^{2+} current and the brief (~15 ms) exponential impulse response function for Ca^{2+} ("kernel" in Figure 5). Therefore, in intact neurons, the kinetics of Ca^{2+} currents play a central role in determining the time course of $[Ca^{2+}]$ signals. This is in contrast to the situation in highly buffered spines in which AP and synaptically evoked $[Ca^{2+}]$ transients have similar time courses (e.g., see Figure 1 and summary of $[Ca^{2+}]$ transient decays in Koester and Sakmann [1998]). Furthermore, our results confirm previous reports that CICR plays no role in synaptically evoked $[Ca^{2+}]$ transients in spines of hippocampal pyramidal neurons (Kovalchuk et al., 2000; Mainen et al., 1999) but is in conflict with the study of Emptage et al. (1999) which found that the majority of synaptically evoked Ca^{2+} influx was due to CICR (discussed in Sabatini et al. [2001]). This contrast may be a result of differences in preparations (whole-cell recordings in acute slices versus sharp recordings in cultured slices) and requires further investigation.

The amplitudes of synaptic $[Ca^{2+}]$ signals in spines are also affected by the presence of Ca^{2+} indicators. We used a combination of methods to determine the amplitudes of NMDA-R mediated $[Ca^{2+}]$ transients at resting and depolarized potentials (Figure 5) under unperturbed conditions. We estimate that the amplitudes of spine $[Ca^{2+}]$ transients following a single synaptic stimulation reach ~12 μM and ~0.7 μM at 0 and −70 mV in unperturbed neurons, respectively.

Compartmentalization of Second Messengers in the Spine

Previous studies of the diffusional coupling of spines and dendrites have used two basic techniques. The first method used fluorescence recovery after photobleaching (FRAP) to measure the diffusional time constants for movement of fluorescent molecules across the spine neck and yielded 20–100 ms for fluorescent dextrans (Svoboda et al., 1996) and 50–800 ms for EGFP (Majewska et al., 2000a). However, because of the high illumina-

tion intensities needed to bleach these fluorophores, photodamage in structures as small as spines is a concern. Photodamage has been shown to retard diffusion in neurons (Koester et al., 1999). Furthermore, how the diffusion of these fluorophores is related to that of Ca^{2+} is not immediately clear. The second method relied on analysis of gradients in the average AP-evoked [Ca^{2+}] transients between spines and the neighboring dendrite to calculate diffusional and extrusion time constants (Majewska et al., 2000b). However, in our experience, in conditions of high exogenous buffer, only a minority of spine/dendrite pairs shows a prolonged [Ca^{2+}] gradient across the spine neck (Figures 2 and 4); thus, most spines are not amenable to this type of analysis. Apparent [Ca^{2+}] gradients between spine head and neighboring dendrite may also be artifacts produced by small errors in the correction for background fluorescence that is often used in the calculation of Ca^{2+} concentrations from fluorescence transients (see Experimental Procedures). Furthermore, in highly buffered conditions, the time constant of Ca^{2+} diffusion across the spine neck and the extrusion time constant of Ca^{2+} across the spine membrane are similar, thereby complicating the interpretation of various decay phases of spine Ca^{2+}.

The fluctuation analysis-based method we used to measure diffusional coupling does not rely on photobleaching nor is its application restricted to spine/dendrite pairs that show large gradients across the spine neck. In fact, we show that even if the average AP-evoked [Ca^{2+}] transients in a spine and its neighboring dendrite are similar in amplitude and time course, the pair is usually diffusionally separated (Figure 4). Thus, as expected from the stochastic nature of VSCC opening, during individual AP-evoked transients, large [Ca^{2+}] gradients may exist across the spine neck. We find that in cells filled with high concentrations of Ca^{2+} indicator, the time constant of equilibration of Ca^{2+} across the spine neck is on average $\sim$90 ms. This is an underestimate of the compartmentalization time of Ca^{2+} in spines of unperturbed cells because of the high mobility of indicators in the cytoplasm relative to that of endogenous Ca^{2+} buffers. In native conditions, the mobility of Ca^{2+} in the cytoplasm is approximately 10- to 100-fold lower than that of Ca^{2+} indicators (Allbritton et al., 1992; Gabso et al., 1997), and diffusional compartmentalization of Ca^{2+} in the spine may persist on the 1–10 s time scale. Thus, under physiological conditions, the spine neck acts as a barrier to diffusion such that the spine head is isolated from the dendrite during the entirety of AP-evoked [Ca^{2+}] transients. Furthermore, Ca^{2+} is compartmentalized even during brief trains of synaptic input, a requirement for the synapse specificity of Ca^{2+}-dependent plasticity mechanisms. In this study, we focused on synapses formed onto identified spines and excluded those made directly onto the dendritic shaft or short, stubby spines. Ca^{2+} accumulations following activation of shaft synapses may have different kinetics and may not show the highly compartmentalized Ca^{2+} handling described above.

Previous studies of Ca^{2+} handling in spines of pyramidal neurons used large quantities of Ca^{2+} indicator and led to the classification of individual spines as "pumpers" if extrusion of Ca^{2+} across the spine membrane was faster than diffusion across the spine neck, or "diffusers" if the opposite was true (Majewska et al., 2000b). We find that such distinctions are not relevant for spines in neurons without added Ca^{2+} buffer. Since Ca^{2+} extrusion is more than 100-fold faster than dissipation by diffusion across the spine neck, the details of spine neck geometry and the time constant of diffusional equilibration play little or no role in determining the kinetics of localized Ca^{2+} signals in the spine. Previously described rapid changes in spine morphology that correlate with changes in the diffusional coupling between the spine and parent dendrite (Majewska et al., 2000a) are also unlikely to affect spine [Ca^{2+}] transients in intact neurons.

The spine neck also poses a barrier to diffusion of other second messengers. For cAMP, cGMP, and IP_3, whose molecular weights (300–1000 D) and diffusion coefficients ($\sim 1 \times 10^{-6}$ cm^2/s) are similar to those of the Ca^{2+} indicator, the equilibration time constant across the spine neck will also be $\sim$100 ms. For these messengers, the variability in spine neck geometry could be important in regulating their passage between spine head and dendrite. Thus modulatory systems that rely on diffusable second messengers and that are differentially activated in spines and dendrites can have spatially restricted effects. This may underlie the selective inhibition of VSCCs in apical spines seen following $GABA_B$ receptor activation in CA1 pyramidal neurons (Sabatini and Svoboda, 2000). Furthermore, movement of proteins will be greatly restricted by the spine neck, and therefore the local accumulation of complexed or enzymatically modified proteins (such as by phosphorylation or cleavage) is possible.

Relevance to Synaptic Plasticity

LTP and LTD are forms of synaptic plasticity that may be the substrates of some forms of long-term memory storage in the brain (Bliss and Collingridge, 1993). LTP is induced by protocols that lead to strong activation of synaptic NMDA-Rs, such as high-frequency afferent activity (Bliss and Collingridge, 1993) or pairing of synaptic stimuli with postsynaptic depolarization (Manabe et al., 1992) or with action potentials (Markram et al., 1997). LTD is induced by protocols that produce relatively weak activation of NMDA-Rs, such as prolonged low-frequency activation (Dudek and Bear, 1992). The salient postsynaptic signal for the induction of both LTP and LTD is the postsynaptic increase of Ca^{2+} (Lisman, 1989; Yang et al., 1999) through NMDA-Rs (Cummings et al., 1996). However, [Ca^{2+}] influx due to postsynaptic action potentials (Markram et al., 1997) and depolarizations (Kullmann et al., 1992) alone is insufficient to induce plasticity. Therefore, the Ca^{2+} signals produced by different stimuli have different biochemical meanings to the cell and lead to divergent physiological responses.

One motivation for our study was to determine how postsynaptic [Ca^{2+}] produced by these different stimuli differs and how they may drive different biochemical cascades. One mechanism could be to directly couple particular Ca^{2+} sensors and Ca^{2+} sources. Close to an open Ca^{2+} channel, Ca^{2+} can reach very high concentrations (>10 μM) (Simon and Llinas, 1985). These "microdomains" of high [Ca^{2+}] exist only within nanometer distances of the channel mouth and dissipate within

microseconds of channel closing. It is thought the Ca^{2+} sensor triggering neurotransmitter release lies within the microdomain of one or more VSCCs. However, it is unlikely that the Ca^{2+} sensor that triggers LTP lies within the microdomain of an NMDA-R. EGTA, a kinetically slow Ca^{2+} chelator that does not interfere with the short-lived microdomains, is able to perturb LTP induction (Lynch et al., 1983), arguing that average spine $[Ca^{2+}]$ is the relevant state variable controlling synaptic plasticity. However, if rises in bulk $[Ca^{2+}]$ in the spine head triggers LTP, how is it that AP-evoked Ca influx is ineffective in triggering synaptic plasticity? Our studies suggest that the explanation may lie in the extremely brief residence time of Ca^{2+} in the cytoplasm following an action potential.

We find that the Ca^{2+} handling mechanisms in spines and distal dendrites are rapid and that bulk $[Ca^{2+}]$ reacts within milliseconds to the opening and closing of Ca^{2+} channels. Thus, although each action potential can generate a large increase in $[Ca^{2+}]$, the rapid clearance of Ca^{2+} from the spine prevents large action potential-evoked $[Ca^{2+}]$ accumulation in the spine even during high-frequency trains (10–100 Hz; Figure 6B). Furthermore, the plateau $[Ca^{2+}]$ level is reached after only five to six spikes, and prolonged trains do not result in further increases in $[Ca^{2+}]$ (Figure 1). On the other hand, NMDA-R-mediated Ca^{2+} accumulation at depolarized potentials following a single synaptic stimulation is large and relatively long lasting (Figures 5D and 6B). Similarly, high Ca^{2+} levels are reached with tetanic stimuli (Petrozzino et al., 1995) and are sufficient to induce LTP (Yang et al., 1999). Reliable induction of LTP also requires maintained ($\sim$2 s) increases in $[Ca^{2+}]$ (Malenka et al., 1992), presumably because of the temporal requirements for full activation of CAMKII (Zucker, 1999). Persistent elevations are unobtainable with action potentials alone but, because of the long-duration of the NMDA-R-mediated Ca^{2+} influx, are easily reached during high-frequency synaptic stimulation.

In contrast, postsynaptic $[Ca^{2+}]$ of less than 1 μM is sufficient to induce LTD (Yang et al., 1999). How is it that action potentials, which raise Ca^{2+} to more than this level, fail to generate LTD? Again, the key difference may be one of kinetics. The induction of LTD is dependent on the activation of protein phosphastase 2B (calcineurin) by calmodulin (Mulkey et al., 1994). Calmodulin must bind four Ca^{2+} ions to be activated, where the binding of the first ion seems to be rate limiting, with an on rate of $\sim$60 $\mu M^{-1}s^{-1}$ and an off rate of $\sim$3 s^{-1} (adjusted for physiological temperatures by a $Q_{10} = 3$ from Holmes [2000]). At $[Ca^{2+}] = 1$ μM, the equilibration time constant for the binding of the first Ca^{2+} ion is $\sim$15 ms. Since AP-evoked $[Ca^{2+}]$ transients remain at high levels only briefly, they will be relatively ineffective at activating calmodulin (Figure 6C) and its downstream effectors, such as calcineurin and CAMKII. The longer NMDA-R-dependent $[Ca^{2+}]$ transient at -70 mV, although of comparable size to the AP-evoked transient, causes a larger peak activation of calmodulin and a vastly greater total activation of calmodulin (Figure 6C). Thus, an intriguing explanation of why LTD can be induced by low-frequency, unpaired synaptic input but not by single or trains of action potentials is that only synaptic $[Ca^{2+}]$ transients can activate kinetically slow Ca^{2+}-dependent processes, such as those that rely on calmodulin activation. The kinetics of Ca^{2+} handling fail to explain the need for prolonged low-frequency stimulation ($\sim$5 min at 1 Hz) (Mulkey and Malenka, 1992) to trigger LTD. Although long-lasting increases in Ca^{2+}, when artificially induced, lead to LTD (Cummings et al., 1996; Yang et al., 1999), we find that in unperturbed neurons, the clearance of Ca^{2+} from the cytoplasm is too rapid to allow Ca^{2+} accumulation during low-frequency stimulation. Thus, the requirement of prolonged stimulation in LTD induction must arise from the accumulation of an effector other than Ca^{2+}.

Experimental Procedures

Electrophysiology

Rat (postnatal day 14–20) hippocampal slices were cut as described previously (Maravall et al., 2000). After cutting, slices were placed in a submerged holding chamber containing ACSF and incubated for 40–60 min at 34°C and then kept at room temperature until use. ACSF contained 127 mM NaCl, 25 mM $NaHCO_3$, 25 mM D-glucose, 2.5 mM KCl, 2 mM $CaCl_2$, 1 mM $MgCl_2$, and 1.25 mM NaH_2PO_4. Experiments were performed at 34°C in ACSF in a submerged recording chamber. In some experiments, one or more of the following drugs were added to the bath solution: 10 μM CPA, 10 μM NBQX, and/or 10 μM bicuculine. Pyramidal neurons in area CA1 were visualized under video IRDIC, and whole-cell recordings were made with 3–5 MΩ electrodes. On break-in, resting potentials were in the range -60 to -70 mV and series resistances were 6–20 MΩ. For current-clamp recordings, electrodes contained 135 mM potassium methylsulfate, 10 mM HEPES, 10 mM sodium phosphocreatine, 4 mM $MgCl_2$, 4 mM Na-ATP, and 0.4 mM Na-GTP. Backpropagating action potentials were induced by somatic current injection (1–3 nA, 2 ms). For voltage-clamp recordings of synaptic transients, cesium methanesulfonate replaced potassium methylsulfate in the internal solution. Electrodes also contained either 20–100 μM Fluo-4, 300 μM Fluo-5F, 20–200 μM Oregon Green 488 BAPTA-1, or 100–200 μM Magnesium Green to monitor calcium levels and either 10–40 μM Alexa Fluor-594 or 100 μM Texas Red to image the neuronal morphology (all from Molecular Probes). For recordings with Magnesium Green, the Cs^+- and K^+-based internal solutions listed above were used with 8 mM CsCl or KCl instead of 4 mM $MgCl_2$. Data acquisition and analysis was performed using custom software written in Igor Pro (Wavemetrics). Summary data are reported as mean $\pm$ SD unless otherwise indicated.

Imaging

We used a custom-built 2-photon laser scanning microscope (2PLSM) (Sabatini and Svoboda, 2000) with an Olympus objective (63×, 0.9 NA), Zeiss scan lens, and a Ti:sapphire laser (Mira, Coherent, Santa Clara, CA) tuned to $\lambda = 810$ nm for excitation. Fluorescence was detected in epifluorescence and transfluorescence (through an oil-immersion condenser, Zeiss, NA = 1.4) modes using photomultiplier tubes (R3896, Hamamatsu, Hamamatsu City, Japan). Image acquisition was controlled by custom software (Ray Stepnoski, Bell Laboratories, Lucent Technologies). In the transfluorescence pathway, a 565 nm dichroic mirror was used to separate green and red fluorescence. BG22 colored glass filters and 607/45 barrier filters were placed respectively in the "green" (shorter wavelength) and "red" (longer wavelength) pathways to eliminate transmitted or reflected excitation light (all filters and dichroics were from Chroma, Brattleboro, VT).

For most experiments, neurons were filled through the patch electrode for 20–40 min before imaging. Red fluorescence was used to locate spines on basal or higher order apical dendrites within 150 μm from the soma (Figures 1A–1D). To measure $[Ca^{2+}]$ changes, green fluorescence was collected while scanning at 500 Hz in a line that intersected both the spine head and its parent dendrite (Figures 1B–1D). Fluorescence was then averaged over the spatial extent of the spine or the dendrite to obtain $F(t)$ for each structure. Baseline fluorescence (F_0) was measured for 50 ms prior to the stimulus and

$\Delta F/F$ was calculated as $(\Delta F/F)(t) = (F(t) - F_0)/F_0$. Calcium concentrations, [Ca^{2+}], were calculated from $\Delta F/F$ using a method that relies on estimating the fluorescence increase that would arise from a saturating Δ[Ca], ($(\Delta F/F)_{max}$) (Maravall et al., 2000). $(\Delta F/F)_{max}$ was calculated from the responses to action potential trains at 62.5 and 83.3 Hz (as in Maravall et al. [2000], Equation 11) (Figure 1) and was used to calculate intracellular [Ca] from $\Delta F/F$ using the equation

$$\frac{\Delta[Ca]}{K_D} = ((\Delta F/F)_{max} + 1) \times (1 - R_f^{-1}) \frac{\Delta F/F}{((\Delta F/F)_{max} - \Delta F/F)(\Delta F/F)_{max}}, \quad (1)$$

where R_f is the dynamic range of the indicator and was measured previously as the ratio of fluorescence from Ca^{2+}-saturated indicator to that from Ca^{2+}-free indicator (Maravall et al., 2000). Because of the weak dependence of $\Delta[Ca]$ on R_f, this method can be used to quantify $\Delta[Ca]$ with good accuracy for indicators with large R_f. Values used were $R_f = 6$ nM and $K_D = 205$ nM for OGB-1 and $R_f = 50$ nM and $K_D = 300$ nM for Fluo-4 (Maravall et al., 2000). Varying the value of R_f for Fluo-4 in range of 25–100 had no significant effect on the results presented here. Only measurements using OGB-1 were used for calculation of resting calcium concentration because Fluo-4 shows little fluorescence under unstimulated conditions.

Synaptic [Ca^{2+}] transients were evoked by positioning a glass extracellular electrode 5–10 μm from a spiny region of dendrite and then adjusting position and stimulus strength until one to two spines in the field of view were stimulated reliably (Mainen et al., 1999). To isolate NMDA-R Ca^{2+} influx, slices were incubated in NBQX and bicuculline. Cells were held in voltage clamp and loaded with 20 μM Alexa-594 and either 100 μM Magnesium Green, to determine the time course of NMDA-R-mediated [Ca^{2+}], or 300 μM Fluo-5F, to determine its amplitude. Recordings were made at either -70 mV or at the reversal potential of the NMDA-R EPSC, (determined separately for each spine, between 0 and 20 mV, and referred to as 0 mV throughout the text and figures). For Fluo-5F, fluorescence increases were calculated as

$$\Delta G/R_{syn} = \frac{(F_{peak}^{green} - F_0^{green})}{F_0^{red}},$$

which is insensitive to the volume of the spine, its location within the slice, and small differences in resting Ca^{2+}. Comparisons of $\Delta G/R_{syn}$ between conditions underestimates the true difference in Ca^{2+} influx because of saturation of Fluo-5F at high Ca^{2+} levels. The affinity of Fluo-5F for Ca^{2+} was determined in cuvettes and found to be 800 nM, with a dynamic range >50.

Reliable determination of [Ca^{2+}] with any method depends critically on accurate measurement of fluorescence from intracellular Ca^{2+} indicator without contamination from other fluorescence sources. In contrast to fura-2 imaging using 340–380 nm excitation, in 2PLSM, there is negligible autofluorescence from the slice ($\sim$1 photon/30 pixels for the excitation levels used in this study). Instead, background fluorescence, when present, is due to fluorescent molecules ejected from the pipette during the process of obtaining a whole-cell recording. Spines are typically substantially smaller than the excitation volume of our microscope (f = spine volume/excitation volume $\sim$10%). Therefore, the volumes and shapes of the spine and excitation kernel, as well as the microscopic distribution of extracellular fluorophores, would need to be known in order to correctly subtract the contribution of extracellular fluorescence sources. For these reasons, it is impractical to correctly convert fluorescence from spines into [Ca^{2+}] or even accurate $\Delta F/F$ in the presence of extracellular fluorescent indicator. Furthermore, performing background correction in the presence of extracellular fluorophores may differentially affect $\Delta F/F$ and [Ca^{2+}] calculated from spines and dendrites. Since the spine typically has a much smaller volume than the parent dendrite, improper background correction will more greatly distort measurements made from the spine.

In the presence of spilled dye, the fluorescence measured from a cellular structure will be

$$F = fI + (1 - f)E,$$

where f is the fraction of the excitation volume occupied by the cellular structure and I and E are the average fluorescence densities inside and outside the structure respectively. If the fluorescence change is calculated with background subtraction as

$$\frac{\Delta F}{F} = \frac{F_1 - F_0}{F_0 - B},$$

where B is the fluorescence measured as background at site away from the structure and is expressed as $B = (1 + \delta(x))E$, where δ is the spatial heterogeneity of the background signal, then

$$\frac{\Delta F}{F} = \frac{f(I_1 - I_0)}{fI_0 + (1 - f)E - B} = \frac{I_1 - I_0}{I_0 - E(1 + \sigma/f)}.$$

Clearly, if $E = 0$, the correct expression for $\Delta F/F$ is obtained. If $E > 0$ and $\delta = 0$, the calculated $\Delta F/F$ will be an underestimate of the true $\Delta F/F$, but the error does not depend on the volume of the structure imaged. However, B is measured at a site away from the imaging site, and thus $\delta \neq 0$ and errors in $\Delta F/F$ will depend on the volume of the structure imaged. Since f is typically <0.2 for spines and small dendrites and often differs by a factor of two to five between the spine and parent dendrite, even small values of δ ($\pm$ 0.1) will introduce large errors in $\Delta F/F$ that differentially affect the spine and the dendrite. These errors can lead to false conclusions about the relative and absolute amplitudes and time courses of [Ca^{2+}] transients in spines and dendrites and can create "overshoots" or "undershoots" in the [Ca^{2+}] transient of the spine relative to that in the dendrite. In addition, calculations of the diffusional coupling between the spine and dendrite and the rates of Ca^{2+} extrusion will be erroneous because of artifactual gradients across the spine neck.

To avoid problems with background subtraction, great care was taken to avoid ejecting dye from the pipette into the slice. Cells in which the surrounding slice showed detectable background fluorescence after dye loading were rejected. Therefore, the only background correction that was performed was subtraction of the photomultiplier tube dark current. This offset was measured with each image acquisition by recording 50 ms prior to shutter opening and specimen illumination.

Measuring Endogenous Buffer Capacity

Calcium buffering capacity was measured by monitoring the amplitude of AP-evoked [Ca^{2+}] transients and was defined as the incremental calcium binding ratio

$$\kappa_X = \frac{K_D^{(x)}[X]_T}{(K_D^{(x)} + [Ca^{2+}]_0)(K_D^{(x)} + [Ca^{2+}]_0 + \Delta[Ca^{2+}]_{AP})}, \quad (2)$$

where κ_X is the buffer capacity of calcium binding species X, $K_D^{(X)}$ is its Ca^{2+} binding affinity, and $[X]_T$ is its total concentration in the cell (Neher and Augustine, 1992). In a neuron that has been filled with Ca^{2+} indicator, the Ca^{2+} buffering is dominated by the endogenous Ca^{2+} buffering capacity of the cell (κ_E) and the Ca^{2+} buffering capacity of the indicator (κ_B). This method relies on rapid (<2 ms) Ca^{2+} equilibration with both endogenous and exogenous Ca^{2+} buffers, and this assumption is supported by the lack of slow endogenous Ca^{2+} buffers in hippocampal pyramidal neurons (Lee et al., 2000a). In a single compartment model (Helmchen et al., 1996), the amplitude of AP-evoked [Ca^{2+}] transients ($\Delta[Ca]_{AP}$) has an inverse dependence on the total buffer capacity, such that

$$\Delta[Ca]_{AP} = \frac{\Delta[Ca]_{TOTAL}}{1 + \kappa_E + \kappa_B}, \quad (3)$$

where $\Delta[Ca]_{TOTAL}$ is the increase in total Ca^{2+} (free and bound) caused by an AP. The single compartment model is applicable here because $\Delta[Ca]_{AP}$ is measured immediately following action potential invasion, before Ca^{2+} can diffuse across the spine neck (Majewska et al., 2000b; Svoboda et al., 1996) (Figure 4). The time constant of decay of Ca^{2+} to resting levels following an AP due to extrusion of Ca^{2+} from the cytoplasm (τ_{decay}) is related to the Ca^{2+} buffering capacity by

$$\tau_{decay} = \frac{1 + \kappa_E + \kappa_B}{\gamma}, \quad (4)$$

where γ is the Ca^{2+} clearance rate. The application of the single

compartment model is gain valid here because of the slow diffusion of Ca^{2+} across the spine neck relative to τ_{decay} and was validated by the quality of the linear fits of Figure 2 and the linear Ca^{2+} extrusion uncovered in Figure 5. To determine the dependence of $\Delta[Ca]_{AP}$ and τ_{decay} on κ_B, both quantities were measured from spines and neighboring dendrites in cells that had been filled to completion with 20 μM Fluo-4 or 20, 50, or 100 μM OGB1. τ_{decay} was also measured in cells filled with 100 μM Magnesium Green. κ_B was measured for each spine/dendrite independently. τ_{decay} was measured with single exponential fits over the first 200 ms of the transient for low buffer capacities and the first 400 ms for high buffer capacities. Fits were constrained to return to the resting Ca^{2+} level measured in the 50 ms prior to action potential initiation. $\Delta[Ca]_{AP}$ was measured from the amplitude of the exponential fit. Fits over longer periods are not possible because photodamage of small structures such as spines during prolonged illumination and are not necessary because of the rapid clearance of Ca^{2+} from distal dendrites and spines. $\Delta[Ca]_{AP}$, τ_{decay}, and κ_B were each averaged across spines for each loading condition to produce the plots in Figure 2, and the relationships between $\Delta[Ca]_{AP}^{-1}$ or τ_{decay} and κ_F were fit by linear regression. The size of AP-evoked [Ca^{2+}] transients in the spine and neighboring dendrite in the absence of indicator can be inferred by extrapolating the fits to $\kappa_B = 0$ (*y* axis intercept). The endogenous calcium buffering capacity (κ_E) was determined from each fit by extrapolating to the *x* axis intercept (Helmchen et al., 1996). 95% confidence intervals were determined using curve-fitting routines and error estimation in Igor Pro (Wavemetrics) and are reported for each value.

Ca^{2+} buffering capacity of individual spines was measured by first briefly filling the neuron with a high concentration of Texas Red (2–3 min, 0.5 mM) then pulling off the neuron. After allowing the neuron to recover (~15 min), a spine was chosen for analysis, and the cell was repatched with a pipette containing only 100 μM OGB-1. $\Delta[Ca]_{AP}$ was monitored in the selected spine and its parent dendrite during filling of the neuron. In other experiments, the patch pipette was tip filled with 100 μM Texas Red and back filled with 100 μM OGB-1. After entering whole-cell mode, a spine was quickly located prior to filling with OGB-1. $\Delta[Ca]_{AP}$ was measured following somatic current injection that generated a single action potential whereas $(\Delta F/F)_{max}$ was determined from AP trains as above. Stimuli were given every 15 s and in the sequence: 3 × 1 AP, 1 × 62.5 Hz train, 3 × 1 AP, and 1 × 83.3 Hz train. $[Ca]_0$ was monitored and cells in which $[Ca]_0$ changed during the OGB-1 loading were not analyzed further (Maravall et al., 2000). In the remaining cells, the concentration of OGB1 during loading was calculated by scaling the pipette concentration of OGB1 by the ratio F_0 at a particular time to F_0 after complete loading of the spine. κ_B was calculated as above, and the relationship between $\Delta[Ca]_{AP}^{-1}$ or τ_{decay} and κ_B was fit by linear regression to determine $\Delta[Ca]_{AP}$, τ_{decay}, and κ_E in unperturbed conditions.

Measuring the Diffusional Equilibration Time Constant

The time constant of equilibration of [Ca^{2+}] across the spine neck was measured with optical fluctuation analysis (Sabatini and Svoboda, 2000). Cells were loaded with 100 μM Fluo-4, and those in which $\Delta[Ca]_{AP}$ was linearly related to $(\Delta F/F)_{AP}$, using the criterion $\Delta[Ca]_{AP} < K_d/5$, were selected. For each spine/dendrite pair, 50–200 trials (0.2 Hz) of action potential-evoked fluorescence transients were recorded. The mean fluorescence transient $\langle F(t)\rangle$ and its variance $\sigma_F^2(t)$ were calculated from the unnormalized fluorescence. The variance in fluorescence due to fluctuations in $\Delta[Ca]_{AP}$ ($\sigma_{F,Ca}^2$) was isolated by subtracting the variance due to dark noise (σ_d^2) and photon shot noise (σ_{sn}^2) from $\sigma_F^2(t)$. Measurements in cuvettes filled with Ca^{2+} indicators ($\sigma_{F,Ca}^2 = 0$) confirmed that σ_{sn}^2 obeys Poisson statistics (i.e., the mean and variance of the number of photons collected are equal) and σ_d^2 was measured by recording 50 ms in each trial prior to shutter opening. Thus,

$$\sigma_{F,Ca}^2(t) = \sigma_F^2(t) - \sigma_d^2 - q\langle F(t)\rangle ,$$

where *q* is the signal produced by the detection of a single photon. Ignoring Ca^{2+} extrusion, in a spine/dendrite pair in which diffusional equilibration across the spine neck occurs with time constant τ_{equi},

$$\frac{dC_{spine}(t)}{dt} = \frac{1}{\tau_{equi}}(C_{dendrite}(t) - C_{spine}(t)) \quad (5)$$

and

$$\frac{d\langle C_{spine}(t)\rangle}{dt} = \frac{1}{\tau_{equi}}(\langle C_{dendrite}(t)\rangle - \langle C_{spine}(t)\rangle) , \quad (6)$$

where C_X and $\langle C_X\rangle$ are the Ca^{2+} concentrations above resting levels in compartment X during a particular trial and on average, respectively. Ca^{2+} is assumed to rise instantaneously at time t = 0 and then equilibrate. Because of the low trial-to-trial variability in the dendrite (Sabatini and Svoboda, 2000),

$$\langle C_{dendrite}\rangle \approx C_{dendrite}. \quad (7)$$

Then, by subtracting Equation 6 from Equation 5 and using the relationship in Equation 7, we get

$$\frac{d(C_{spine} - \langle C_{spine}\rangle)}{dt} = \frac{1}{\tau_{equi}}(C_{spine} - \langle C_{spine}\rangle) ,$$

and solving the differential equation yields

$$C_{spine}(t) - \langle C_{spine}(t)\rangle =$$

$$(C_{spine}(0) - \langle C_{spine}(0)\rangle)e^{-t/\tau_{equi}},$$

with $\langle C_{spine}(\infty)\rangle \approx C_{spine}(\infty)$, since the steady-state level will be determined by influx into the entire cell and has little or no trial-to-trial variability. Then the variance is given by

$$\sigma_{C_{spine}}^2(t) = \sigma_{C_{spine}}^2(0)e^{-2t/\tau_{equi}}.$$

Under conditions in which fluorescence is linearly related to [Ca],

$$\sigma_{F,Ca,spine}^2(t) = \sigma_{F,Ca,spine}^2(0)e^{-2t/\tau_{equi}}.$$

and, therefore, the decay time constant of the variance (τ_{var}) in the spine is related to the decay time constant of diffusional equilibration (τ_{equi}) by $\tau_{equi} = 2\tau_{var}$. Errors due to ignoring Ca^{2+} extrusion make τ_{equi} measured by this method an underestimate of the true τ_{equ}. τ_{var} was measured from single exponential fits to the measured $\sigma_{F,Ca,spine}^2(t)$ (Figures 4C and 4D).

Acknowledgments

We thank J. Lisman, M. Maravall, T. Pologruto, and R. Yasuda for helpful comments on the manuscript and B.J. Burbach and P. O'Brien for technical assistance. This work was supported by fellowships from the Helen Hay Whitney (B.S.) and Swartz (T.O.) Foundations, the NIH, and the Mathers, Pew, and Klingenstein Foundations (K.S.).

Received July 18, 2001; revised November 28, 2001.

References

Allbritton, N.L., Meyer, T., and Streyer, L. (1992). Range of messenger action of calcium ion and inositol 1,4,5-trisphosphate. Science *258*, 1812–1815.

Andersen, P., Sundberg, S.H., Sveen, O., Swann, J.W., and Wigstrom, H. (1980). Possible mechanisms for long-lasting potentiation of synaptic transmission in hippocampal slices from guinea-pigs. J. Physiol. *302*, 463–482.

Bito, H., Deisseroth, K., and Tsien, R.W. (1997). Ca^{2+}-dependent regulation in neuronal gene expression. Curr. Opin. Neurobiol. *7*, 419–429.

Bliss, T.V.P., and Collingridge, G.L. (1993). A synaptic model of memory: long-term potentiation in the hippocampus. Nature *361*, 31–39.

Cummings, J.A., Mulkey, R.M., Nicoll, R.A., and Malenka, R.C. (1996). Ca^{2+} signaling requirements for long-term depression in the hippocampus. Neuron *16*, 825–833.

Dudek, S.M., and Bear, M.F. (1992). Homosynaptic long-term depression in area CA1 of hippocampus and effects of N-methyl-D-aspartate receptor blockade. Proc. Natl. Acad. Sci. USA *89*, 4363–4367.

Emptage, N., Bliss, T.V.P., and Fine, A. (1999). Single synaptic events

evoke NMDA receptor-mediated release of calcium from internal stores in hippocampal dendritic spines. Neuron *22*, 115–124.

Engert, F., and Bonhoeffer, T. (1999). Dendritic spine changes associated with hippocampal long-term synaptic plasticity. Nature *399*, 66–70.

Fierro, L., and Llano, I. (1996). High endogenous calcium buffering in Purkinje cells from rat cerebellar slices. J. Physiol. *496*, 617–625.

Fischer, M., Kaech, S., Wagner, U., Brinkhaus, H., and Matus, A. (2000). Glutamate receptors regulate actin-based plasticity in dendritic spines. Nat. Neurosci. *3*, 887–894.

Gabso, M., Neher, E., and Spira, M.E. (1997). Low mobility of the Ca^{2+} buffers in axons of cultured Aplysia neurons. Neuron *18*, 473–481.

Guerini, D., and Carafoli, E. (1999). The calcium pumps. In Calcium as a Cellular Regulator, E. Carafoli and C. Klee, eds. (New York: Oxford University Press), pp. 249–278.

Harris, K.M., and Kater, S.B. (1994). Dendritic spines: cellular specializations imparting both stability and flexibility to synaptic function. Annu. Rev. Neurosci. *17*, 341–371.

Helmchen, F., Imoto, K., and Sakmann, B. (1996). Ca^{2+} buffering and action potential-evoked Ca^{2+} signaling in dendrites of pyramidal neurons. Biophys. J. *70*, 1069–1081.

Hollingworth, S., Zhao, M., and Baylor, S.M. (1996). The amplitude and time course of the myoplasmic free [Ca^{2+}] transient in fast-twitch fibers of mouse muscle. J. Gen. Physiol. *108*, 455–469.

Holmes, W.R. (1990). Is the function of spines to concentrate calcium? Brain Res. *519*, 338–342.

Holmes, W.R. (2000). Models of calmodulin trapping and CaM kinase II activation in a dendritic spine. J. Comput. Neurosci. *8*, 65–85.

Jaffe, D.B., Johnston, D., Lasser, R.N., Lisman, J.E., Miyakawa, H., and Ross, W.N. (1992). The spread of Na^{+} spikes determines the pattern of dendritic Ca^{2+} entry into hippocampal neurons. Nature *357*, 244–246.

Kennedy, M.B. (2000). Signal-processing machines at the postsynaptic density. Science *290*, 750–754.

Koch, C., and Zador, A. (1993). The function of dendritic spines: devices subserving biochemical rather than electrical compartmentalization. J. Neurosci. *13*, 413–422.

Koester, H.J., and Sakmann, B. (1998). Calcium dynamics in single spines during coincident pre- and postsynaptic activity depend on relative timing of back-propagating action potentials and subthreshold excitatory postsynaptic potentials. Proc. Natl. Acad. Sci. USA *95*, 9596–9601.

Koester, H.J., and Sakmann, B. (2000). Calcium dynamics associated with action potentials in single nerve terminals of pyramidal cells in layer 2/3 of the young rat neocortex. J. Physiol. *529*, 625–646.

Koester, H.J., Baur, D., Uhl, R., and Hell, S.W. (1999). Ca^{2+} fluorescence imaging with pico- and femtosecond two-photon excitation: signal and photodamage. Biophys. J. *77*, 2226–2236.

Kovalchuk, Y., Eilers, J., Lisman, J., and Konnerth, A. (2000). NMDA receptor-mediated subthreshold Ca^{2+} signals in spines of hippocampal neurons. J. Neurosci. *20*, 1791–1799.

Kullmann, D.M., Perkel, D.J., Manabe, T., and Nicoll, R.A. (1992). Ca2+ entry via postsynaptic voltage-sensitive Ca^{2+} channels can transiently potentiate excitatory synaptic transmission in the hippocampus. Neuron *9*, 1175–1183.

Lee, S.H., Schwaller, B., and Neher, E. (2000a). Kinetics of Ca^{2+} binding to parvalbumin in bovine chromaffin cells: implications for [Ca^{2+}] transients of neuronal dendrites. J. Physiol. *525 Pt 2*, 419–32.

Lee, S.-H., Rosenmund, C., Schwaller, B., and Neher, E. (2000b). Differences in Ca buffering properties between excitatory and inhibitory hippocampal neurons from the rat. J. Physiol. *525 Pt 2*, 405–418.

Lisman, J. (1989). A mechanism for the Hebb and the anti-Hebb processes underlying learning and memory. Proc. Natl. Acad. Sci. USA *86*, 9574–9578.

Lynch, G., Larson, J., Kelso, S., Barrionuevo, G., and Schottler, F. (1983). Intracellular injections of EGTA block induction of hippocampal long-term potentiation. Nature *305*, 719–721.

Maeda, H., Ellis-Davies, G.C., Ito, K., Miyashita, Y., and Kasai, H. (1999). Supralinear Ca^{2+} signaling by cooperative and mobile Ca^{2+} buffering in Purkinje neurons. Neuron *24*, 989–1002.

Mainen, Z.F., Malinow, R., and Svoboda, K. (1999). Synaptic calcium transients in single spines indicate that NMDA receptors are not saturated. Nature *399*, 151–155.

Majewska, A., Tashiro, A., and Yuste, R. (2000a). Regulation of spine calcium dynamics by rapid spine motility. J. Neurosci. *20*, 8262–8268.

Majewska, A., Brown, E., Ross, J., and Yuste, R. (2000b). Mechanisms of calcium decay kinetics in hippocampal spines: role of spine calcium pumps and calcium diffusion through the spine neck in biochemical compartmentalization. J. Neurosci. *20*, 1722–1734.

Malenka, R.C., and Nicoll, R.A. (1999). Long-term potentiation—a decade of progress? Science *285*, 1870–1874.

Malenka, R.C., Lancaster, B., and Zucker, R.S. (1992). Temporal limits on the rise in postsynaptic calcium required for the induction of long-term potentiation. Neuron *9*, 121–128.

Maletic-Savatic, M., Malinow, R., and Svoboda, K. (1999). Rapid dendritic morphogenesis in CA1 hippocampal dendrites induced by synaptic activity. Science *283*, 1923–1927.

Manabe, T., Renner, P., and Nicoll, R.A. (1992). Postsynaptic contribution to long-term potentiation revealed by the analysis of miniature synaptic currents. Nature *355*, 50–55.

Maravall, M., Mainen, Z.M., Sabatini, B., and Svoboda, K. (2000). Estimating intracellular calcium concentrations and buffering without wavelength ratioing. Biophys. J. *78*, 2655–2667.

Markram, H., Luebke, J., Frotscher, M., and Sakmann, B. (1997). Regulation of synaptic efficacy by coincidence of postsynaptic APs and EPSPs. Science *275*, 213–215.

Miyakawa, H., Lev-Ram, V., Lasser-Ross, N., and Ross, W.N. (1992). Calcium transients evoked by climbing fiber and parallel fiber synaptic inputs in guinea pig cerebellar Purkinje neurons. J. Neurophysiol. *68*, 1178–1189.

Mulkey, R.M., and Malenka, R.C. (1992). Mechanisms underlying induction of homosynaptic long-term depression in area CA1 of the hippocampus. Neuron *9*, 967–975.

Mulkey, R.M., Endo, S., Shenolikar, S., and Malenka, R.C. (1994). Involvement of a calcineurin/inhibitor-1 phosphatase cascade in hippocampal long-term depression. Nature *369*, 486–488.

Neher, E., and Augustine, G.J. (1992). Calcium gradients and buffers in bovine chromaffin cells. J. Physiol. *450*, 273–301.

Petrozzino, J.J., Miller, L.D.P., and Connor, J.A. (1995). Micromolar Ca^{2+} transients in dendritic spines of hippocampal pyramidal neurons in brain slice. Neuron *14*, 1223–1231.

Philipson, K. (1999). Sodium-calcium exchange. In Calcium as a Cellular Regulator, E. Carafoli and C. Klee, eds. (New York: Oxford University Press), pp. 249–278.

Sabatini, B.L., and Svoboda, K. (2000). Analsyis of calcium channels in single spines using optical fluctuation analysis. Nature *408*, 589–593.

Sabatini, B.S., Maravall, M., and Svoboda, K. (2001). Ca^{2+} signaling in spines. Curr. Opin. Neurobiol. *11*, 349–356.

Simon, S.M., and Llinas, R.R. (1985). Compartmentalization of the submembrane calcium activity during calcium influx and its significance in transmitter release. Biophys. J. *48*, 485–498.

Spacek, J., and Harris, K.M. (1997). Three-dimensional organization of smooth endoplasmic reticulum in hippocampal CA1 dendrites and dendritic spines of the immature and mature rat. J. Neurosci. *17*, 190–203.

Storm, J.F. (1990). Potassium currents in hippocampal pyramidal cells. Prog. Brain Res. *83*, 161–187.

Svoboda, K., Tank, D.W., and Denk, W. (1996). Direct measurement of coupling between dendritic spines and shafts. Science *272*, 716–719.

Tank, D.W., Regehr, W.G., and Delaney, K.R. (1995). A quantitative analysis of presynaptic calcium dynamics that contribute to short term enhancement. J. Neurosci. *15*, 7940–7952.

Toni, N., Buchs, P.A., Nikonenko, I., Bron, C.R., and Muller, D. (1999).

LTP promotes formation of multiple spine synapses between a single axon terminal and a dendrite. Nature *402*, 421–425.

Wang, S.S., Denk, W., and Hausser, M. (2000). Coincidence detection in single dendritic spines mediated by calcium release. Nat. Neurosci. *3*, 1266–1273.

Yang, S.N., Tang, Y.G., and Zucker, R.S. (1999). Selective induction of LTP and LTD by postsynaptic $[Ca^{2+}]_i$ elevation. J. Neurophysiol. *81*, 781–787.

Yuste, R., and Denk, W. (1995). Dendritic spines as basic functional units of neuronal integration. Nature *375*, 682–684.

Yuste, R., Majewska, A., Cash, S.S., and Denk, W. (1999). Mechanisms of calcium influx into hippocampal spines: heterogeneity among spines, coincidence detection by NMDA receptors, and optical quantal analysis. J. Neurosci. *19*, 1976–1987.

Zucker, R.S. (1999). Calcium- and activity-dependent synaptic plasticity. Curr. Opin. Neurobiol. *9*, 305–313.